Chemical Engineering Science 64 (2009) 2941 – 2950

Contents lists available at ScienceDirect

Chemical Engineering Science

journal homepage: www.elsevier.com/locate/ces

On the CFD modelling of Taylor flow in microchannels

Raghvendra Gupta, David F. Fletcher*, Brian S. Haynes

School of Chemical and Biomolecular Engineering, The University of Sydney, Sydney, NSW, Australia

ARTICLE INFO

Article history:
Received 22 October 2008
Received in revised form 5 March 2009
Accepted 9 March 2009
Available online 26 March 2009

Keywords:
Taylor bubble
Microchannels
Multiphase flow
CFD
Mesh resolution
Liquid film
Contact angle

ABSTRACT

With the increasing interest in multiphase flow in microchannels and advancement in interface capturing techniques, there have recently been a number of attempts to apply computational fluid dynamics (CFD) to model Taylor flow in microchannels. The liquid film around the Taylor bubble is very thin at low Capillary number (*Ca*) and requires careful modelling to capture it. In this work, a methodology has been developed to model Taylor flow in microchannel using the ANSYS Fluent software package and a criterion for having a sufficiently fine mesh to capture the film is suggested. The results are shown to be in good agreement with existing correlations and previous valid modelling studies. The role played by the wall contact angle in Taylor bubble simulations is clarified.

1. Introduction

With the advancement in microfabrication techniques, the use of micro-structured devices has gained importance in a range of industrial applications. High surface-area-to-volume ratio and the small diffusion paths in such devices make them ideal candidates for heat exchangers and microreactors. The laminar nature of the flow in microchannels helps in efficient design of the micro-structured devices as no heuristic model is required to model laminar flow. Multiphase flow can further enhance the performance of these microfluidic devices by providing large interfacial area (Günther and Jensen, 2006). As a result, recently there has been an enormous interest in the study of two-phase adiabatic and non-adiabatic gas–liquid flow in microchannels (Suo and Griffith, 1964; Barnea et al., 1983; Damianides and Westwater, 1988; Barajas and Panton, 1993; Fukano and Kariyasaki, 1993; Mishima et al., 1993; Bao et al., 1994; Mishima and Hibiki, 1996; Triplett et al., 1999; Bao et al., 2000; Zhao and Bi, 2001; Chen et al., 2002; Kawahara et al., 2002; Serizawa et al., 2002; Cubaud and Ho, 2004; Pehlivan et al., 2006; Saisorn and Wongwises, 2008).

Depending upon the properties and flow rates of the two fluids, various flow patterns such as bubbly, slug or Taylor, churn, rivulet, wavy annular, annular flow etc. occur in gas–liquid flow in microchannels. Taylor flow (also known as slug flow, Taylor bubble flow, bubble-train flow, intermittent flow, plug flow etc.) is one of the most important flow patterns and occupies a large area on the flow-regime map (Triplett et al., 1999). Taylor flow is characterised by gas bubbles that almost fill the channel, separated by liquid slugs. A thin liquid film separates these bubbles from the wall and also connects the two successive liquid slugs separated by the gas bubble. Due to the recirculating flow in the liquid slugs, Taylor flow improves heat and mass transfer from the liquid to the wall. This flow pattern also provides a large interfacial area and thus enhances gas–liquid mass transfer. The separation of liquid slugs by the bubble also reduces axial liquid mixing. Thus, enhanced radial mass transfer and reduced axial mass transfer make Taylor flow suitable for applications which suffer from large back-mixing (Angeli and Gavriilidis, 2008).

Due to its interesting flow characteristics, the Taylor flow regime has received enormous attention over the years and has been studied experimentally, analytically and using computational fluid dynamics (CFD). Recently, there has been some confusion regarding the existence of the liquid film surrounding the gas bubble in various CFD modelling efforts to study Taylor flow. While some researchers acknowledge that the liquid film was not captured because a sufficiently refined grid was not used (Qian and Lawal, 2006; Yu et al., 2007), others have carried out CFD simulations showing dry walls (no liquid film present with the gas bubble in direct contact with the wall) assuming it to be a physically acceptable result and go on to study the effect of wall contact angle on fully developed Taylor flow (He et al., 2007; Kumar et al., 2007).

This work reviews the occurrence of wall dry-out during experimental studies and compares the observed regime with those described in numerical studies. It is shown that numerical issues, such as grid refinement, need careful attention when modelling Taylor

* Corresponding author.
E-mail address: d.fletcher@usyd.edu.au (David F. Fletcher).

0009-2509/$ - see front matter © 2009 Elsevier Ltd. All rights reserved.
doi:10.1016/j.ces.2009.03.018

flow in microchannels and unphysical results are readily produced if sufficient care is not taken. A detailed study of the effect of various numerical practices is then presented and results are compared with widely accepted correlations.

2. Literature review

Two-phase flow regimes in microchannels have been investigated experimentally by various researchers. With the exception of stratified flow, the major flow patterns that are common in macrochannels occur in microchannels, although certain flow pattern details may be different from those in large channels. Fig. 1 shows the frequently cited flow-regime map of Triplett et al. (1999) which was developed for air–water two-phase flow in a horizontal circular channel of 1.45 mm inner diameter in gas superficial velocity (U_{GS}) versus liquid superficial velocity (U_{LS}) coordinates. Five main flow regimes were identified, as shown in Fig. 1, namely bubbly, slug, churn, slug-annular and annular flow. This flow regime map is in good agreement with those reported by other researchers (Mishima and Hibiki, 1996; Coleman and Garimella, 1999; Yang and Shieh, 2001; Chen et al., 2002; Chung and Kawaji, 2004; Pehlivan et al., 2006; Ide et al., 2007), with discrepancies generally due to a different description of the regimes. The present work is concerned with slug or Taylor flow and dry-out at the wall, and this review therefore focuses on Taylor flow and cases where wall dry-out was reported. Fig. 2 shows representative pictures of the slug flow pattern as observed by Triplett et al. (1999) in a 1.1 mm channel. This flow pattern has been referred to as slug (Suo and Griffith, 1964), plug (Damianides and Westwater, 1988) or bubble-train flow (Thulasidas et al., 1997).

Barajas and Panton (1993) determined the flow patterns visually in 1.6 mm horizontal channels of four different materials having different contact angles for an air–water system. Different flow patterns, such as wavy-stratified, plug, slug, annular, bubbly, rivulet etc. were observed in their experiments. Plug flow was similar to Taylor flow as defined here, while slug flow was defined as a flow pattern containing intermittent slugs of liquid blocking the entire channel cross-section. The observed flow patterns were quite similar to those observed in large diameter horizontal channels (Hewitt and Hall-Taylor, 1970; Coleman and Garimella, 1999).

Zhao and Bi (2001) investigated the air–water two-phase flow patterns in vertical equilateral triangular section channels with hydraulic diameters of 2.89, 1.44 and 0.87 mm. It was noted that, in the channel of smallest dimension, a capillary bubbly flow pattern, characterised by a train of ellipsoidal-shaped bubbles spanning almost the entire channel cross-section, led to the side-walls being partially dry at low liquid flow rates.

Serizawa et al. (2002) studied air–water two-phase flow in round tubes of 20–100 μm and observed different flow patterns, such as dispersed bubbly flow, gas slug flow, liquid ring flow, liquid lump flow, skewered barbecue (Yakitori) shaped flow, annular flow and rivulet flow. They also pointed out that dry and wet areas existed between the gas slug and tube wall at low velocities.

Cubaud and Ho (2004) carried out experimental investigations of gas–liquid two-phase flow in 200 and 500 μm square-section microchannels. In the experiments, dewetting was observed in two flow-regimes, named wedge flow and dry flow. In wedge flow they state: "For a partially wetting system, as a function of the bubble velocity, bubbles can dry out the center of the channel creating triple lines (liquid/gas/solid). The liquid film between the gas and the center of the channel can be considered as static, while liquid flows in the corner." This partial dry-out of the channel walls is similar to that observed by Zhao and Bi (2001) in triangular microchannels. The dry flow occurs when the homogeneous void fraction is more than 0.995 and the liquid flow is restricted to the corners of the channel.

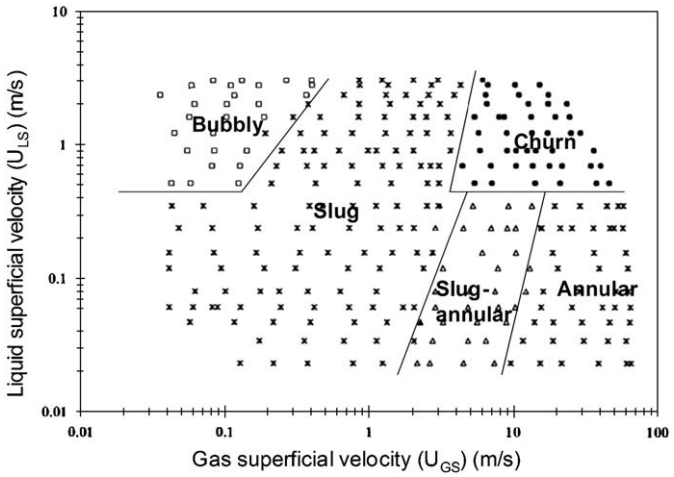

Fig. 1. Flow pattern map as observed by Triplett et al. (1999) for a 1.45 mm diameter circular test section. The transition lines are only indicative and are not from Triplett et al.

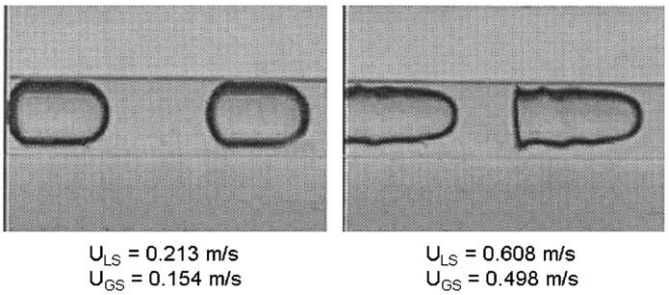

Fig. 2. Representative photograph of Taylor or slug flow in a 1.1 mm circular microchannel as observed by Triplett et al. (1999).

Taylor flow has also been studied numerically by using different approaches. Earlier studies assumed a bubble shape and simulated the flow around the bubble using a free-slip boundary condition at the bubble interface. For example, van Baten and Krishna (2004, 2005) simulated the flow in the liquid domain around the bubble and also studied mass transfer from Taylor bubbles to the liquid phase. They showed that a very fine grid (cell size smaller than 1 μm for a channel of 3 mm diameter) was required to capture the steep concentration gradients near the bubble surface and in the liquid film. Giavedoni and Saita (1997, 1999) analysed numerically the liquid flow field in the leading front and the rear part of a long bubble separately by using a finite element method which allowed the bubble interface to move. Kreutzer et al. (2005) also used a finite element method to simulate the flow around the bubble allowing the bubble interface to move.

The flow of Taylor bubbles has also been studied extensively in large diameter vertical channels in the past, for example Taha and Cui (2002), Bugg and Saad (2002) and Ndinisa et al. (2005). Ndinisa et al. (2005) studied the flow of Taylor bubbles in a vertical tubular membrane of diameter 19 mm using different models: VOF, Eulerian two-fluid, and a model that used a solution-adapted dispersed-phase length-scale, using ANSYS CFX-5.6. Simulations results were compared with the experimental data of Bugg and Saad (2002) and were found to be in reasonable agreement. A uniform square grid of size 0.25 mm was used in the simulations. It was noted that an extremely fine mesh is required to properly resolve such flows.

With advances in multiphase flow modelling, various interface-capturing techniques have been used to model Taylor flow in

microchannels: the volume-of-fluid (VOF) approach (Qian and Lawal, 2006), the level-set method (Fukagata et al., 2007), or the phase-field method (He et al., 2007; He and Kasagi, 2008). Commercial CFD codes such as ANSYS Fluent and CFD-ACE+, as well as specialised in-house codes have been used for the modelling. Commercial codes that use the VOF method, often incorporate geometric reconstruction schemes (e.g. the PLIC scheme of Youngs, 1982) to capture the gas–liquid interface. Recently, Fletcher et al. (2009) reviewed CFD modelling of microchannel flows and pointed out that the main challenges in the modelling of multiphase flow in microchannels are the correct identification of the interface location and the occurrence of parasitic currents arising from the modelling of surface tension (Lafaurie et al., 1994; Harvie et al., 2006).

Taha and Cui (2004) modelled Taylor flow in a vertical capillary for a two-dimensional, axisymmetric geometry using Fluent. A computational domain of length of 11 diameters having a grid of size 26×280 was used for the simulations, with the grid being refined near the wall. The flow field was solved in a reference frame moving with the bubble. A constant velocity was specified at the inlet and outflow boundary condition was used at the outlet. The results of the simulations, such as bubble velocity, diameter and velocity field around the bubble were found to be in good agreement with experimental data.

Qian and Lawal (2006) used Fluent to model Taylor bubble formation in a T-junction microchannel for a two-dimensional planar geometry with a cross-sectional width ranging from 0.25 to 3 mm. The gas and liquid were fed from the two different legs of the T-junction. The effect of inlet configuration, gas and liquid flow rates and properties on the slug length was studied. The length of the flow domain was 60 tube diameters and the computational mesh contained only 6600 elements which is too coarse to capture the details of the flow. It was remarked, "Unfortunately, our grid resolution is not fine enough to capture the liquid film". However, the results were found to be in surprisingly good agreement with the experimental data and this work is cited in numerous articles that use similarly coarse meshes.

Fukagata et al. (2007) modelled two-dimensional, axisymmetric, periodic Taylor bubble flow and heat transfer (without phase change) in a 20 μm tube using the level-set method (Sussman et al., 1994). The void fraction, pressure gradient, bubble period and wall heat flux were used as input parameters. The bubble shape and the flow field around it were calculated and used to determine the gas and liquid superficial velocities and the two-phase frictional multiplier. They compared their results with the experimental data of Serizawa et al. (2002) and found reasonable agreement between the two. They also noticed that the bubble period has a considerable influence on the flow pattern.

He et al. (2007) carried out two-dimensional axisymmetric numerical simulations of gas–liquid two phase flow in a channel having a radius of 10 μm and a length of 40 μm using the phase-field method. A periodic boundary condition with specified pressure drop was applied in the streamwise direction. A square grid was used with 32 elements in the radial direction. Void fraction, pressure drop and initial velocity (either zero or a parabolic velocity profile) and an assumed bubble shape were used as the input. The final bubble shape and the superficial velocities of the gas and liquid were calculated in the simulation. The results showed that the final gas–liquid interface could be wall-contacting (dry) or non-wall contacting (wet) depending on the input conditions. The dry-out conditions were said to be similar to those observed in the experiments by Serizawa et al. (2002) and Cubaud and Ho (2004). However, as mentioned earlier, dry-out at the wall in the experiments of Serizawa et al. (2002) was observed at low velocities, which is not the case in the numerical simulations. The dry-out mentioned by Cubaud and Ho (2004) is either typical of non-circular polygonal channels or occurs for a homogeneous void fraction greater than 0.995, conditions which did not obtain in the simulations.

Yu et al. (2007) studied gas–liquid flow in rectangular microchannels experimentally and numerically. The numerical study was carried out using the Lattice–Boltzmann method. The liquid film was successfully captured at capillary numbers (based on liquid properties) of 0.03 or above. However, the film could not be captured successfully at lower values of capillary number ($Ca < 0.02$). It was noted that this failure in capturing the liquid film could be attributed to the limited resolution of the simulations. They also pointed out, "When dry patches are formed, the flow problem becomes much more complicated, with complex moving contact lines and small droplets and bubbles sticking to the wall. This poses tremendous challenges for numerical simulation and cannot be solved by increasing the spatial resolution alone."

Kumar et al. (2007) studied Taylor flow numerically in curved microchannels of diameters ranging from 0.25 to 3 mm. A mesh-independence study was carried out for four different mesh densities. The study showed that the gas–liquid interface became sharp as the mesh was refined, which is a direct outcome of using a refined mesh in the streamwise direction. However, the liquid film on the wall was not captured by even the finest mesh used, because the radial mesh was not refined sufficiently. The effect of inlet geometry, channel diameter, curvature ratio, inlet volume fraction, surface tension, liquid viscosity and wall contact angle on slug length was studied. However, it is not possible to place any reliance on these results as the hydrodynamics changes significantly with the presence of liquid film on the wall.

Kashid et al. (2008) studied the hydrodynamic characteristics of liquid–liquid slug flow experimentally using the micro-PIV technique and computationally using interface capturing CFD techniques. A wall film surrounding the bubble was observed during the experiments. The computational studies were carried out using both the VOF and level-set methods. It was noted that the fine mesh size was one thousandth of the slug diameter. However, the wall film was not captured in the simulations. They also carried out single phase simulations by assuming the fixed interface position obtained from experimental data.

Carlson et al. (2008) compared the performance of Fluent and TransAT, a high accuracy CFD code, for the simulation of multiphase flow in microchannels in the slug flow regime. The simulations in Fluent were carried out using VOF with the high order CISAM scheme used to maintain the interface sharp, while in TransAT the level-set method was used to capture the gas–liquid interface. Two-dimensional, axisymmetric simulations were carried out in a channel of 1 mm diameter and 30 mm length. The gas and liquid velocities were defined at the inlet as a uniform velocity profile. Numerical dry-out (break up of the liquid film on the tube wall, with gas in direct contact with the solid surface) was observed in the simulations using Fluent and the mesh near the wall needed to be refined to avoid the numerical dry-out. The bubble shape at low gas–liquid flow rates was found to be similar but the bubble frequency and the flow fields obtained from the two codes were different. At high gas–liquid flow rates, Fluent failed to capture the gas–liquid interface correctly. The authors pointed out that a similar deficiency in capturing the interface at a low gas–liquid flow rate was observed when the convergence criteria were relaxed. It was also observed that the choice of time integration scheme did not affect the results significantly.

Lakehal et al. (2008) also used TransAT to perform a two-dimensional, axisymmetric CFD analysis of multiphase flow and heat transfer in circular horizontal miniature tube of diameter 1 mm, using the level-set method. The flow was modelled for a fixed liquid flow rate and different gas flow rates in the slug flow regime. By grid and domain sensitivity studies, it was shown that a channel

length of 40 diameters was required to achieve a quasi-steady state (or a fully-developed flow) for multiphase flow and around 900 grid elements in the axial direction were required to resolve the flow features. It was concluded that the slug flow regime in two-phase flow regime in microchannels can be modelled successfully and qualitatively, with the flow topology captured being similar to experimental observations.

Chen et al. (2009) carried out unsteady, two-dimensional, axisymmetric simulations of Taylor bubble flow in a vertical channel of diameter 1 mm and length 5–10 mm using the level-set method. At the inlet, a co-flow nozzle arrangement (including nozzle wall) was used to inject air and octane. The fully developed circular and annular channel velocity profiles were specified for the gas and liquid, respectively. At the nozzle wall, no penetration and the Navier-slip conditions ($u_{slip} = -\lambda(\partial u/\partial y)_{wall}$, where λ is the slip length) were specified for the normal and tangential velocity components, respectively. At the outlet, either outflow or a fully developed velocity profile with a mean velocity equal to inlet two-phase velocity was specified. Both of the outlet boundary conditions gave similar results until the bubble reached the outlet. A contact line model was applied to consider the effect of hysteresis and the dynamic nature of the contact angle at the nozzle wall. The grid spacing used in the simulation was 1/60th of the channel diameter. The results were compared with the experimental data of Salman et al. (2006) and found to be in good agreement. It was noted that the formation of Taylor bubbles was mainly dependent on the relative magnitudes of the gas and liquid superficial velocities for a given nozzle/tube configuration. However, a change in nozzle geometry could change the size of the Taylor bubbles and pressure drop significantly for the same superficial velocities.

Fang et al. (2008) studied the evolution of liquid slug flow with sidewall liquid injection in rectangular microchannels experimentally and numerically. A model was proposed to include the wall adhesion forces by considering the effect of contact angle hysteresis and it was demonstrated that the model including hysteresis effect predicted the liquid slug detachment in excellent agreement with those measured in the experiments. It was also shown that the results were quite different when a constant contact angle was used in the model. This study shows that the effect of dynamic contact angle needs to be modelled accurately to capture the slug growth and detachment behaviour at the wall in the injector region.

Liu and Wang (2008) investigated upward Taylor flow in vertical square and equilateral triangular capillaries of hydraulic diameter 1 mm and length 16 mm using Fluent. A fully developed velocity profile was set at the inlet and an outflow boundary condition was used at the outlet. The simulations were carried out in a reference frame moving with the bubble. The liquid inlet velocity was iteratively adjusted until the position and shape of the bubble were stable in the domain. The bubble size and shape, film thickness and velocity field were studied as a function of Capillary number.

Although not directly related to Taylor bubbles, the numerical study of droplet behaviour in a sudden contraction by Rosengarten et al. (2006) highlights the role the contact angle can play when the film surrounding the "bubble" becomes very thin and can be influenced by long range van der Waal forces. Both experimental and computational results are used to illustrate the effect of contact angle for very thin films.

The above review of the literature on two-phase gas–liquid flow in microchannels shows that:

- Taylor bubble flow has been observed as an important flow regime in the experimental studies to establish flow-regime maps of gas–liquid flow in microchannels.
- The bubbles are almost always surrounded by the liquid. Dry-out at the wall has been observed under only very particular conditions, such as non-circular geometries or very high homogeneous void fraction ($\beta > 0.995$). This dry-out on the wall is a three-dimensional phenomenon and requires the use of three dimensional modelling that includes a dynamic contact angle model.
- Numerous numerical studies have been carried out to model Taylor flow in microchannels. The liquid film at the wall has not been captured successfully in many of these studies due to poor resolution of the flow near the wall. This deficiency of the numerical simulation has a profound effect on frictional pressure drop and heat and mass transfer to the wall. Capturing the liquid film is crucial in the numerical modelling of Taylor flow.
- Some researchers believe that the wall adhesion properties, such as wall contact angle, play an important role in Taylor flow modelling. This is not entirely true. The role of the wall contact angle is only important when both of the fluids are in contact with the wall or the film is so thin that van der Waal forces can act across the film. This may be the case in T or Y type junctions where both phases remain in contact with the wall but once a Taylor bubble flow is obtained with a liquid film at the wall, wall adhesion plays no role in determining the bubble shape. Moreover, the modelling of wall adhesion requires inclusion of the contact angle hysteresis effect to obtain meaningful results.

3. Mathematical modelling

The usual approach to the modelling of multiphase flow in microchannels is to compute the evolution of the gas–liquid interface (Hessel et al., 2004). This can be achieved by using a "single-fluid" formulation in which a common flow field is shared by all of the phases. The hydrodynamics of such flows can be described by the equations for the conservation of mass and momentum, together with an additional advection equation to determine the gas–liquid interface. For an incompressible, Newtonian fluid, these equations can be written as follows:

Continuity:

$$\frac{\partial \rho}{\partial t} + \nabla.\rho\mathbf{V} = 0 \tag{1}$$

Momentum:

$$\frac{\partial(\rho\mathbf{V})}{\partial t} + \nabla.(\rho\mathbf{V}\otimes\mathbf{V}) = -\nabla p + \nabla.(\mu(\nabla\mathbf{V} + \nabla\mathbf{V}^{\mathbf{T}})) + \mathbf{F_s} \tag{2}$$

Volume fraction:

$$\frac{\partial \alpha}{\partial t} + \mathbf{V}.\nabla\alpha = 0 \tag{3}$$

where $\mathbf{V}$ denotes the velocity vector, p the pressure, ρ the density and μ the dynamic viscosity of the fluid. $\mathbf{F_s}$ is the surface tension force approximated as a body force in the vicinity of the interface, and α is the volume fraction of one of the phases. The bulk properties, such as density and viscosity, are determined from the volume-fraction weighted average of the properties of the two fluids.

In the present work, the flow field has been calculated using a two-dimensional, axisymmetric (cylindrical) geometry in order to save computational time and effort. The effect of gravity has been neglected as it plays a minor role in multiphase flow in microchannels (Triplett et al., 1999). Fig. 3 shows a schematic of the channel and the boundary conditions applied. At the inlet, the gas enters at the core and the liquid enters as an annulus around the gas core. Plug flow of the gas and the liquid is assumed. At the outlet, a constant area-averaged pressure boundary condition is applied. The usual no-slip boundary condition is applied at the wall and a zero normal gradient boundary condition for all the variables is applied on the axis.

Fig. 3. Schematic representation of the geometry and boundary conditions used in the simulations.

4. Solution methodology

The Fluent commercial CFD software is used to model two-dimensional, axisymmetric, transient, two-phase Taylor flow in a microchannel. This section describes the details of various numerical schemes used.

4.1. VOF Method

The volume-of-fluid method (Hirt and Nichols, 1981) is used to identify the gas–liquid interface by solving a volume fraction equation (Eq. (3) above) for one of the phases. An explicit geometric reconstruction scheme is used to represent the interface by using a piecewise-linear approach (Youngs, 1982). The time step used for the VOF equation in Fluent is not necessarily the same as that used for the other equations but is calculated based upon the characteristic transit time of a fluid element across a control volume and is limited by a specified maximum value for the Courant number. The time taken to empty a cell is calculated by dividing the volume of each cell by the sum of the outgoing fluxes in the region near the fluid interface. The smallest such time is used as the characteristic time of transit for a fluid element across a control volume. The Courant number (Co) is defined by Eq. (4) as

$$Co = \frac{\Delta t}{\Delta x / V_{\text{fluid}}} \tag{4}$$

where Δx is the grid size and V_{fluid} is the fluid velocity. A maximum Courant number of 0.25 is set in the present calculations and a variable time step based on a fixed Courant number of 0.25 or less was used to force the time step to be the same for all the equations.

4.2. Surface tension model

The continuum surface force (CSF) model proposed by Brackbill et al. (1992) is used to model surface tension effects. The CSF model approximates the surface tension-induced stress by a body force, which acts throughout a small but finite fluid region surrounding the interface. The surface tension force per unit area is represented as

$$\mathbf{F_s} = \sigma\kappa\delta(\mathbf{r} - \mathbf{r}_{\text{int}})\mathbf{n} \tag{5}$$

where σ is the coefficient of surface tension, $\boldsymbol{\kappa}$ is the radius of curvature, $\delta(\mathbf{r})$ is the Dirac delta function and $\mathbf{n}$ denotes the unit normal vector on the interface. The normal $\mathbf{n}$ and curvature $\boldsymbol{\kappa}$ in Eq. (5) are defined in terms of the volume fraction (α) via:

$$\mathbf{n} = \frac{\nabla\alpha}{|\nabla\alpha|} \tag{6}$$

and

$$\kappa = \nabla.\mathbf{n} \tag{7}$$

This implementation of the surface tension force can induce unphysical velocity near the interface known as 'spurious currents' (Lafaurie et al., 1994; Harvie et al., 2006). This occurs because the pressure and viscous force terms do not exactly balance the surface tension force. The accurate calculation of gradients can help in minimising these spurious currents.

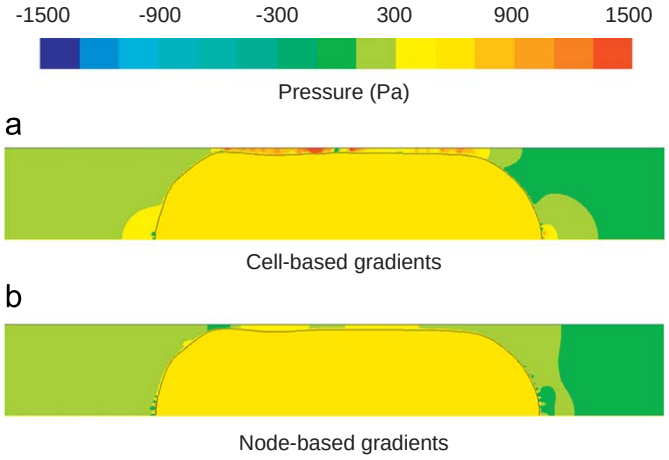

Fig. 4. Pressure distribution after ~7.1 ms for (a) Green–Gauss node-based gradients (b) Green–Gauss cell-based gradients for a 100×2000 mesh and $U_{LS} = 0.255$ m/s and $U_{GS} = 0.245$ m/s. The simulations for the two cases were started using the same initial conditions. The bubble interface is shown by a black line.

A contact angle of 90° was specified in all cases. In Fluent the contact angle is used to adjust the surface normal in cells near the wall and therefore sets the curvature of the interface near the wall. Given that there is no gas–solid–liquid interface present at the inlet or when Taylor bubbles are present this model should not have any effect on the results. However, as we will see later it determines the "bubble" shape in poorly resolved simulations.

In Fluent the gradient of scalars (pressure, velocity components and volume fraction) must be calculated at the cell centre from the scalar values at the cell face centroids. Two different methods, namely Green–Gauss cell-based and Green–Gauss node-based, are available to calculate the cell face centroid values of scalars for structured meshes. In cell-based calculations, the cell face centroid values are computed from the arithmetic average of the values at the neighbouring cell centres, whilst in node-based calculations, cell face centroid values are computed by the arithmetic average of the nodal values on the faces. The nodal values are computed from the weighted average of the cell values surrounding the nodes. It is worth emphasising here that the gradients are computed at the cell centres for both cell-based and node-based gradient calculations. Fig. 4 shows the pressure contour around a bubble for calculations using the Green–Gauss cell-based and node-based gradient methods. Both the cases were run using the same discretization and numerical schemes and were started using the same initial condition. In the cell-based gradient case, significant unphysical pressure oscillations are observed in the liquid film near the bubble interface. These result in a very erratic velocity field in the film. It is evident from the figure that using node-based gradients helps to minimise these unphysical oscillations, although small unphysical pressure oscillation still remain at the head and tail of the bubble.

4.3. Solver options

An implicit body force treatment (for the surface tension force in the present case) is used to take into account the partial equilibrium of the pressure gradient and body forces, as recommended in Fluent 6.3.26 Users' Guide (2006). Fluent uses a co-located scheme in which pressure and velocity are stored at the cell centres. However, the calculation of pressure gradients requires the pressure values to be interpolated from cell centres to the cell faces. In the present computations, a body-force-weighted interpolation scheme is used

Table 1
Properties of the gas and the liquid used in the simulations.

Fluid	Density (kg/m^3)	Viscosity ($kg/m\,s$)	Surface tension (N/m)
Water	997	8.899×10^{-4}	0.072
Air	1.185	1.831×10^{-5}	

to compute the face pressure by assuming that the normal gradient of the difference between the pressure and body forces is constant.

A first order, non-iterative fractional step scheme is used for the time marching of the momentum and continuity equations. The correction tolerances for sub-iterations (the ratio of the residuals at the current sub-iteration and the first sub-iteration) for pressure and momentum equations used are 0.01 and 0.001, respectively. The residual tolerance for both the equations was set to 0.0001. The specified values of correction tolerances are much lower than the default values of 0.25 for the pressure equation and 0.05 for the momentum equations. The absolute values of residuals achieved were found to be sufficiently low ($O(10^{-8})$ for velocities and $O(10^{-10})$ for continuity) using these correction and residual tolerances that the results were unaffected by the level of convergence achieved. A variable time step (Δt), based on a fixed Courant number of 0.25, is used for the momentum and pressure equations. The QUICK scheme is used for the discretisation of the momentum equations.

5. Results and discussion

A circular channel of diameter 0.5 mm and length of 10D is used in the present calculations. Air and water are used as the working fluids. The properties of the working fluids are listed in Table 1. The flow conditions are chosen to have a low Capillary number and consequently a thin film so that the issue of film capture can be highlighted. The superficial velocities (phase volumetric flow rate per unit channel cross-sectional area) of the gas and the liquid are 0.245 and 0.255 m/s, respectively, and the void fraction at the inlet is equal to the homogeneous void fraction. These flow conditions correspond to Ca and Re values of 0.006 and 280, respectively.

5.1. Grid-independence study

This section demonstrates the importance of proper grid resolution in the CFD modelling of Taylor flow in microchannels. The surface tension force is applied at the cell centre and is calculated from the gradient of volume fraction. Therefore, having a structured square grid (cubic in the case of a three-dimensional grid) in the region where the gas–liquid interface is present is beneficial to minimise inaccuracies in the calculation of the surface tension force. In the best practice guidelines for the modelling of multiphase flow using Fluent, Barbat (2004) also states that a square grid should be used for flows involving surface tension forces.

Fig. 5 shows the liquid volume fraction plot for different grids having element sizes ranging from 25 μm (D/20) to 5 (D/100) μm in a channel of length 10D. The gas–liquid interface becomes sharp and the air slug length independent of the grid size upon grid refinement. This gives the illusion of having attained a grid-independent solution. The gas liquid interface is normal to the wall, as dictated by the chosen contact angle of 90°. More realistic looking bubble shapes could be obtained by changing the contact angle but this apparent improvement would be a purely numerical artefact. Some of the finer grids were able to capture the liquid film successfully at the start of the channel. However, none of these grids was able to maintain the liquid film as the bubble moved forward. For example, the 5 μm grid is able to capture the liquid film initially but the film is disrupted as the bubble moves forward. Fig. 6 shows the liquid volume fraction

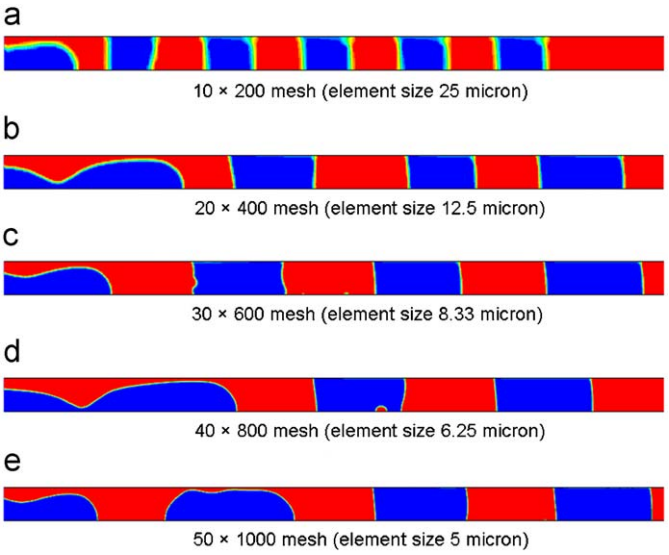

Fig. 5. Plots of liquid volume fraction for five different meshes. The results for different meshes are at different time instants. The air is coloured blue and the water is coloured red. (For interpretation of the references to colour in this figure legend, the reader is referred to the web version of the article.)

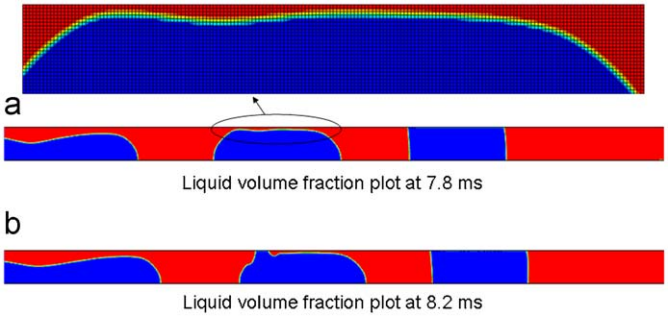

Fig. 6. Liquid volume fraction plot for a 5 μm size mesh at (a) 7.8 ms and (b) 8.2 ms. In Fig. 6(a), an enlarged view of the grid in the liquid film is also shown. The air is coloured blue and the water is coloured red. (For interpretation of the references to colour in this figure legend, the reader is referred to the web version of the article.)

plot for 5 μm size grid at two different time instants: the first when the liquid film is present around the second bubble and the second when it is disrupted. The enlarged view of the near-film region in Fig. 6(a) shows that only two elements are present in the film. This grid resolution is clearly not sufficient to capture the complex flow field around the bubble and the grid needs further refinement.

Fig. 7 compares the results obtained using computational grids having uniform element sizes of 5 μm (D/100), 2.5 μm (D/200) and 1.67 μm (D/300). Fig. 7(a) shows that the finer grids of element size 2.5 and 1.67 μm are able to capture the liquid film successfully. However, the ultra-refined grids are not only computationally expensive but they also cause increased non-physical pressure jumps across the interface, arising from the use of high order discretisation, on refinement as shown in Fig. 7(b). The pressure field plot for the 5 μm grid (Fig. 7(bi)) shows that the entire pressure field changes on disruption of liquid film at the wall.

A guide for the determination of a sufficiently fine near-wall mesh to capture the liquid film at the wall can be given based on the above results. Angeli and Gavriilidis (2008) reviewed data on Taylor bubbles in micro-channels. Based on their review we use the film thickness (δ) correlation given by Bretherton (1961) to calculate the

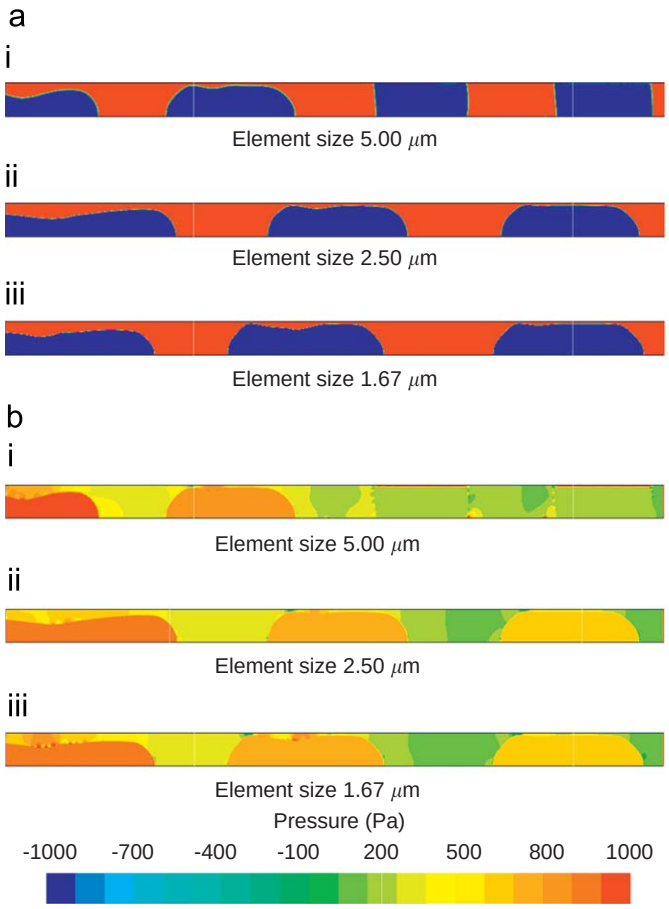

Fig. 7. (a) Liquid volume fraction plot for uniform fine grids. The air is coloured blue and the water is coloured red and (b) pressure contour plot for uniform fine grids. The results for different meshes are at different time instants. (For interpretation of the references to colour in this figure legend, the reader is referred to the web version of the article.)

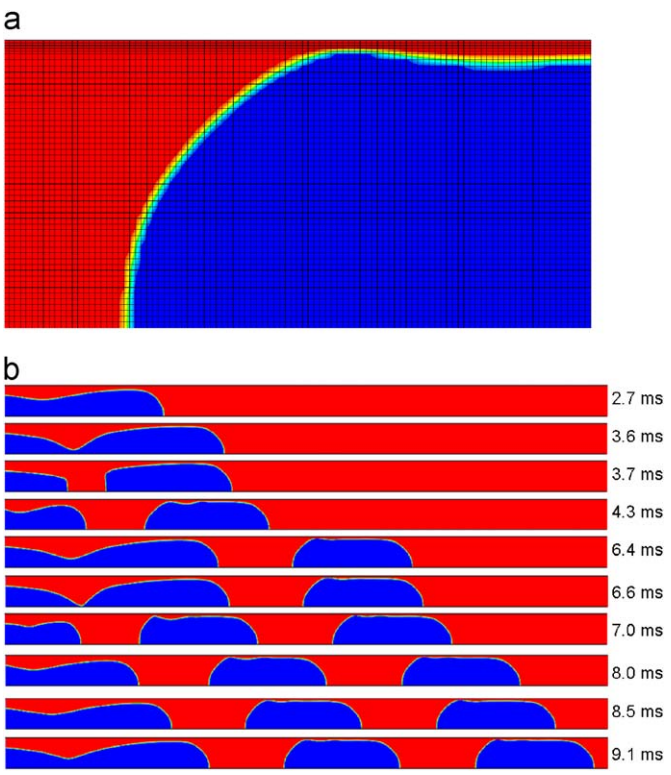

Fig. 8. (a) Refined mesh near the wall in the liquid film region and (b) process of bubble formation and reshaping with time. The liquid is shown in red and the gas in blue. (For interpretation of the references to colour in this figure legend, the reader is referred to the web version of the article.)

approximate film thickness. This gives

$$\frac{\delta}{R} = 1.34Ca^{2/3} \tag{8}$$

where the Capillary number Ca is defined via

$$Ca = \frac{\mu_L(U_{LS} + U_{GS})}{\sigma} \tag{9}$$

μ_L is the viscosity of the liquid and U_{LS} and U_{GS} are the superficial velocities of the liquid and the gas, respectively. From our observations, a minimum of five elements are needed across the liquid film and so the minimum suitable mesh size can be calculated using the above correlation. In the current case the liquid film thickness calculated from Eq. (8) is 12 μm and therefore a grid size of 2.4 μm should be able to capture the liquid film successfully.

The simulations were run on a HP workstation having two Pentium4 processors (3 GHz each) and 3 GB of RAM. The 5, 2.5 and 1.67 μm grid simulations took an average of 1.6, 5 and 14 s per timestep for a serial run, respectively. As the grid is refined, the time step also becomes smaller (for a fixed value of the Courant number) and so the simulations on very fine grids are very costly, taking typically 13 days for the finest mesh. Therefore, to address the two conflicting requirements of having a uniform square grid in the region where the gas–liquid interface is present and sufficient near wall fine mesh to capture the liquid film, a grid (shown in Fig. 8a) having uniform square elements of size 5 μm in the core and rectangular elements (2.4 μm×5 μm) in the 12 μm thick film region was used for the simulations. Using this grid the liquid film was captured successfully and the coarser grid near the axis also helped in minimising the pressure oscillations at the interface. In the next section, the results obtained with this grid (unless specified otherwise) have been compared with those obtained from empirical correlations available in the literature.

5.2. Analysis

Fig. 8(b) shows the process of bubble evolution with time. The air bubble grows and fills up almost the entire channel (2.7 ms). Necking occurs at around 3.6 ms and the bubble then breaks off (3.7 ms). After break-off, the bubble shape becomes bullet-like (6.4 ms) and then moves forward without any change in the shape (6.6 ms and onwards). A small undulation is observed at the rear of the bubble interface. This is similar to the simulation results of the rear meniscus of a long bubble by Giavedoni and Saita (1999). Taha and Cui (2004) also predicted a similar bubble shape for a Capillary number (Ca) of 0.007 in a vertical capillary. Some very small amplitude waves are observed at the film-bubble interface. The process of bubble separation is periodic and the length and shape of the first and second bubbles are similar. Therefore, the flow properties can be analysed in a unit cell which consists of a single bubble and two halves of the adjacent liquid slugs.

5.2.1. Film thickness

Table 2 compares the numerically calculated film thickness (determined far enough downstream of the inlet that the film thickness is no longer changing) with the film thickness obtained using various empirical correlations. The film thickness calculated by established

Table 2
A comparison of the liquid film thickness between the simulation results and available correlations for Taylor flow in horizontal microchannels.

Relationship for δ/R	Film thickness (δ) (μm)
$0.5Ca^{1/2}$ (Fairbrother and Stubbs, 1935; Taylor, 1960)	10
$1.34Ca^{2/3}$ (Bretherton, 1961)	11
$\frac{1.34Ca^{2/3}}{1+2.5(1.34Ca^{2/3})}$ (Aussillous and Quere, 2000)	10
Present computations (5 μm near wall fine grid)	15
Present computations (2.5 μm grid)	12
Present computations (1.67 μm grid)	12

correlations is $0.04R$ and the film thickness obtained by the finest grids in the present computations is $0.05R$. The film thickness calculated using two ultra-fine grids showed that a grid independent film thickness was obtained.

5.2.2. Gas hold-up

The Armand correlation (Armand and Treschev, 1946) given by Eq. (10) has been widely used and found to predict the gas hold-up (the void fraction or the volume fraction of the gas) in Taylor flow regime in microchannels well (Chung and Kawaji, 2004). It gives

$$\varepsilon_G = 0.833\beta \tag{10}$$

where $\beta(=U_{GS}/(U_{LS}+U_{GS}))$ is the homogeneous void fraction. For the present case the gas hold-up calculated using the Armand correlation is 0.41. In the simulations, the gas hold-up is calculated by dividing the volume of the air bubble by that of the unit-cell (consisting of a gas bubble and two halves of liquid slugs) volume. The value obtained is 0.455, which differs by 10% from the correlation value.

5.2.3. Bubble length and velocity

The length of the bubble is dependent on the inlet configuration and a change in the inlet configuration can cause a significant change in the bubble length. In the present case, the length of the bubble is $2.0D$ and the slug length is $1.3D$, defined at the centreline.

The steady bubble velocity (U_B) in a horizontal microchannel can be calculated using

$$U_B = \frac{U_{GS}}{\varepsilon_G} \tag{11}$$

The bubble velocity obtained from Eqs. (11) is 0.54 m/s. The bubble velocity in the present computations is calculated as the velocity of bubble nose and gives a value of 0.55 m/s. This is within 2% of the exact value, suggesting that the flow is very close to being fully developed.

5.2.4. Pressure distribution in a unit-cell

Fig. 9(a) shows the pressure distribution in a unit-cell at 8.5 ms. The pressure in the liquid slug and gas bubble region is different largely due to the interfacial pressure together with a contribution from dynamic head. The interfacial pressure difference in the constant film region is of the order of σ/R (290 Pa), while the interfacial pressure difference in the bubble nose region is of the order of $2\sigma/R$ (580 Pa). However, the large radius of curvature at the rear interface of the bubble causes the interfacial pressure difference to be less than $2\sigma/R$. There is a small low pressure zone near the interface undulation at the rear of the bubble. A minimum in pressure is observed at the rear of bubble. This is similar to the pressure field observed by Kreutzer et al. (2005) for $Ca = 0.004$ and $Re = 500$. Fig. 9(b) shows the pressure variation along the axis and the wall. The pressure in the gas bubble is constant while the pressure in the liquid region ahead of the bubble shows a monotonic decrease with distance, which is

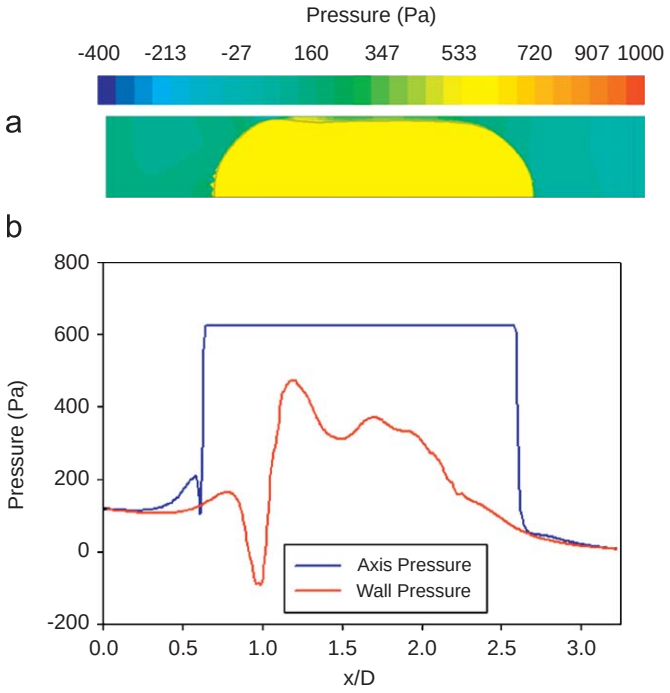

Fig. 9. Pressure distribution at 8.5 ms. (a) Pressure contour plot in the unit cell. The bubble interface and unit cell boundaries have been shown by black lines. (b) Variation of pressure on the axis and along the wall for a unit cell.

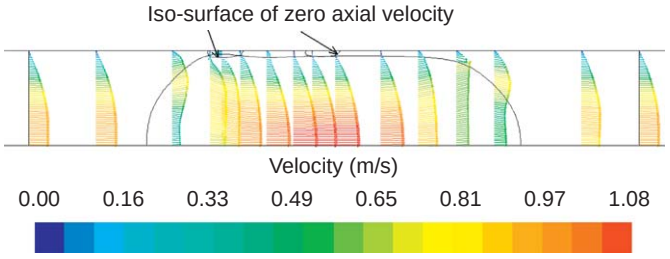

Fig. 10. Flow field velocity vectors coloured by velocity magnitude in a unit cell at 8.5 ms. The iso-surfaces of zero axial velocity is also shown. The bubble interface and unit cell boundaries are shown by black lines.

consistent with the developing flow, as can be seen in Fig. 10. The pressure profile in the slug region behind the bubble is more complex, with significantly different pressures at the wall and the axis close to the bubble. There are clearly numerical effects at the tail of the bubble but these have only a localised influence, as the velocity profile again appears similar to that in developing flow (Fig. 10).

For a unit-cell the computed pressure drop is 70,700 Pa/m. Kreutzer et al. (2005) suggested a correlation for the friction factor for Taylor bubbles in small-diameter tubes of the form

$$f = \frac{16}{Re}\left[1 + \alpha_1 \frac{D}{L_S}\left(\frac{Re}{Ca}\right)^{1/3}\right] \tag{12}$$

where L_S is the slug length, $Re = D(U_{LS} + U_{GS})\rho_L\mu_L$ is the Reynolds number and α_1 is a constant. The value of α_1 was found to be 0.07 and 0.17 for numerical simulations and experimental data, respectively. The difference in the value was attributed to the presence of impurities at the interface. Based on the above friction factor correlation, the pressure drop per unit length can be calculated by the

following equation

$$\frac{\Delta P}{L} = \varepsilon_L f \left(\frac{4}{D}\right)\left(\frac{1}{2}\rho_L (U_{LS}+U_{GS})^2\right) \quad (13)$$

where ε_L is the dynamic liquid hold-up. The pressure drop per unit length for the present case is calculated from Eqs. (12) and (13) to be 94,400 and 184,000 Pa/m using the numerical and experimental values of α_1, respectively. The computed pressure drop in the present calculations is close to that obtained using the numerically obtained value of α_1.

5.2.5. Flow field

Fig. 10 shows the velocity vectors in and around the bubble in a unit cell at a time of 8.5 ms. A recirculation zone exists in the liquid film near the undulation at the back of the bubble with another forming ahead of it. The iso-surfaces of zero axial velocity show the locations of the recirculation zones in the figure. These recirculation zones extend into the gas bubble.

6. Conclusions

A review of Taylor flow in horizontal microchannels with a focus on the existence or not of a liquid film at the wall was carried out and it is concluded that:

- Taylor bubbles are always surrounded by the liquid and the dry-out at the walls is observed only under very particular conditions, such as during transient mixing of gas and liquid from separate streams, flow in non-circular geometries or at very high homogeneous void fraction.
- The liquid film at the wall has not been captured successfully in many numerical studies performed to model Taylor flow, largely due to the poor near-wall resolution. This has a profound effect on the predicted hydrodynamics.
- Wall adhesion properties (contact angle) play a role only when the gas and liquid are both in contact with the wall i.e. a three phase contact line exists, which is generally the case only at the inlet where the bubbles are formed. Modelling of wall adhesion phenomena requires inclusion of contact angle hysteresis effect to obtain any meaningful results. However, in poorly resolved simulations that do not capture the presence of a liquid film, the use of a small contact angle leads to the appearance of a rounded bubble even when the gas is contacting the wall (see for e.g. Qian and Lawal, 2006 who used a contact angle of 0°).

A methodology has been developed to simulate Taylor flow in horizontal microchannels using the VOF method. Various challenges have been identified and the ways to address these challenges have been suggested:

- The continuum surface force model used to model surface tension generates spurious currents near the gas–liquid interface. The most accurate gradient calculation and the use of grid elements of aspect ratio unity help in minimising the errors in surface tension modelling.
- A guideline based on the Capillary number (Ca) to create the near wall grid has been developed to determine the mesh size required to capture the liquid film successfully.
- The present simulations captured the broad flow features as observed in experiments and predicted the liquid film thickness, void fraction, bubble velocity and pressure drop in good agreement with the available correlations.

The methodology can be easily used to model the flow in non-circular cross-sections and complex channel paths. It can also be extended to model heat and mass transfer in Taylor flow.

Notation

Ca	Capillary number ($=\mu_L(U_{LS}+U_{GS})/\sigma$)
Co	Courant number
D	channel diameter, m
f	friction factor
$\mathbf{F_s}$	surface tension force, N/m^3
L	unit cell length, m
L_s	slug length, m
$\mathbf{n}$	normal vector to the interface
p	static pressure, Pa
ΔP	pressure drop, Pa
$\mathbf{r}$	location vector, m
$\mathbf{r}_{int}$	location vector at the interface, m
R	channel radius, m
Re	Reynolds number ($=D(U_{LS}+U_{GS})\rho_L\mu_L$)
t	time, s
Δt	time step, s
u_{slip}	slip velocity, m/s
U_B	bubble velocity, m/s
U_{GS}	gas superficial velocity, m/s
U_{LS}	liquid superficial velocity, m/s
$\mathbf{V}$	velocity, m/s
V_{fluid}	fluid velocity, m/s
Δx	grid size, m

Greek letters

α	volume fraction of a phase
α_1	empirical constant
β	homogeneous void fraction
δ	film thickness, m
$\delta(\mathbf{r})$	dirac-delta function
ε_G	gas hold-up
ε_L	dynamic liquid hold-up
κ	radius of curvature, m^{-1}
λ	slip length, m
μ	mixture viscosity, kg/m s
μ_L	liquid viscosity, kg/m s
ρ	mixture density, kg/m^3
ρ_L	liquid density, kg/m^3
σ	coefficient of surface tension, N/m

Acknowledgements

RG acknowledges the University of Sydney's Henry Bertie and Florence Mabel Gritton research scholarship foundation. This work was supported by an Australian Research Council (ARC) Discovery Grant (DP0559516).

References

Angeli, P., Gavriilidis, A., 2008. Hydrodynamics of Taylor flow in small channels: a review. Proceedings of IMechE: Part C: Mechanical Engineering Science 222, 737–751.

Armand, A.A., Treschev, G.G., 1946. The resistance during the movement of a two-phase system in horizontal pipes. Izvestya Vsesoyuznogo Teplotekhnicheskogo Instituta 1, 16–23.

Aussillous, P., Quere, D., 2000. Quick deposition of a fluid on the wall of a tube. Physics of Fluids 12 (10), 2367–2371.

Bao, Z.Y., Bosnich, M.G., Haynes, B.S., 1994. Estimation of void fraction and pressure drop for two-phase flow in fine passages. Transactions on IChemE, Part A, Chemical Engineering Research and Design 72, 625–632.

Bao, Z.Y., Fletcher, D.F., Haynes, B.S., 2000. An experimental study of gas–liquid flow in a narrow conduit. International Journal of Heat and Mass Transfer 43, 2313–2324.

Barajas, A.M., Panton, R.L., 1993. The effect of contact angle on two-phase flow in capillary tubes. International Journal of Multiphase Flow 19, 337–346.
Barbat, T., 2004. Best practices for modelling multiphase flows in automotive industry. Fluent Automotive Users' Group Meeting, ⟨http://www.fluentusers.com⟩.
Barnea, D., Luninski, Y., Taitel, Y., 1983. Flow in small diameter pipes. Canadian Journal of Chemical Engineering 61, 617–620.
Brackbill, J.U., Kothe, D.B., Zemach, C., 1992. A continuum method for modeling surface tension. Journal of Computational Physics 100 (2), 335–354.
Bretherton, F.P., 1961. The motion of long bubbles in tubes. Journal of Fluid Mechanics 10, 166–188.
Bugg, J.D., Saad, G.A., 2002. The velocity field around a Taylor bubble rising in a stagnant viscous fluid: numerical and experimental results. International Journal of Multiphase Flow 28 (5), 791–803.
Carlson, A., Kudinov, P., Narayanan, C., 2008. Prediction of two-phase flow in small tubes: a systematic comparison of state-of-the-art CMFD codes. In: Proceedings: Fifth European Thermal-Sciences Conference, Eindhoven, Netherlands.
Chen, W.L., Twu, M.C., Pan, C., 2002. Gas–liquid two-phase flow in micro-channels. International Journal of Multiphase Flow 28 (7), 1235–1247.
Chen, Y., Kulenovic, R., Mertz, R., 2009. Numerical study on the formation of Taylor bubbles in capillary tubes. International Journal of Thermal Sciences 48 (2), 234–242.
Chung, P.M.Y., Kawaji, M., 2004. The effect of channel diameter on adiabatic two-phase flow characteristics in microchannels. International Journal of Multiphase Flow 30 (7–8), 735–761.
Coleman, J.W., Garimella, S., 1999. Characterization of two-phase flow patterns in small diameter round and rectangular tubes. International Journal of Heat and Mass Transfer 42 (15), 2869–2881.
Cubaud, T., Ho, C.M., 2004. Transport of bubbles in square microchannels. Physics of Fluids 16 (12), 4575–4585.
Damianides, C.A., Westwater, J.W., 1988. Two-phase flow patterns in a compact heat exchanger and in small tubes. In: Proceedings of Second UK National Conference on Heat Transfer, Glasgow, Glasgow, Mechanical Engineering Publications, London.
Fairbrother, F., Stubbs, A.E., 1935. The bubble-tube method of measurement. Journal of Chemical Society 1, 527–529.
Fang, C., Hidrovo, C., Wang, F.M., Eaton, J., Goodson, K., 2008. 3-D numerical simulation of contact angle hysteresis for microscale two phase flow. International Journal of Multiphase Flow 34 (7), 690–705.
Fletcher, D.F., Haynes, B.S., Aubin, J., Xuereb, C., 2009. Modelling of microfluidic devices. In: Hessel, V., Schouten, J.C., Renken, A., Yoshida, J.-I. (Eds.), Handbook of Micro Reactors, Fundamentals, Operations and Catalysts, vol. 1. Wiley-VCH, pp. 117–144 (Chapter 5).
Fluent 6.3.26 Users' Guide, 2006. Fluent Inc., Lebanon, NH, 2006.
Fukagata, K., Kasagi, N., Ua-arayaporn, P., Himeno, T., 2007. Numerical simulation of gas–liquid two-phase flow and convective heat transfer in a micro tube. International Journal of Heat and Fluid Flow 28 (1), 72–82.
Fukano, T., Kariyasaki, A., 1993. Characteristics of gas–liquid two-phase flow in a capillary tube. Nuclear Engineering and Design 141 (1–2), 59–68.
Giavedoni, M.D., Saita, F.A., 1997. The axisymmetric and plane cases of a gas phase steadily displacing a Newtonian liquid—a simultaneous solution of the governing equations. Physics of Fluids 9 (8), 2420–2428.
Giavedoni, M.D., Saita, F.A., 1999. The rear meniscus of a long bubble steadily displacing a Newtonian liquid in a capillary tube. Physics of Fluids 11 (4), 786–794.
Günther, A., Jensen, K.F., 2006. Multiphase microfluidics: from flow characteristics to chemical and material synthesis. Lap on a Chip 6, 1487–1503.
Harvie, D.J.E., Davidson, M.R., Rudman, M., 2006. An analysis of parasitic current generation in Volume of Fluid simulations. Applied Mathematical Modelling 30 (10), 1056–1066.
He, Q., Fukagata, K., Kasagi, N., 2007. Numerical simulation of gas–liquid two-phase flow and heat transfer with dry-out in a micro tube. In: Proceedings: Sixth International Conference on Multiphase Flow, Leipzig, Germany.
He, Q., Kasagi, N., 2008. Phase-field simulation of small capillary-number two-phase flow in a microtube. Fluid Dynamics Research 40 (7–8), 497–509.
Hessel, V., Hardt, S., Lowe, H., 2004. Chemical Micro Process Engineering-Fundamentals, Modelling and Reactions. Wiley-VCH, Weinheim.
Hewitt, G.F., Hall-Taylor, N.S., 1970. Annular Two-Phase Flow. Pergamon Press Ltd., Oxford.
Hirt, C.W., Nichols, B.D., 1981. Volume of Fluid (VOF) method for the dynamics of free boundaries. Journal of Computational Physics 39, 201–225.
Ide, H., Kariyasaki, A., Fukano, T., 2007. Fundamental data on the gas–liquid two-phase flow in minichannels. International Journal of Thermal Sciences 46 (6), 519–530.
Kashid, M.N., Rivas, D.F., Agar, D.W., Turek, S., 2008. On the hydrodynamics of liquid–liquid slug flow capillary microreactors. Asia-Pacific Journal of Chemical Engineering 3 (2), 151–160.
Kawahara, A., Chung, P.M.Y., Kawaji, M., 2002. Investigation of two-phase flow pattern, void fraction and pressure drop in a microchannel. International Journal of Multiphase Flow 28 (9), 1411–1435.
Kreutzer, M.T., Kapteijn, F., Moulijn, J.A., Kleijn, C.R., Heiszwolf, J.J., 2005. Inertial and interfacial effects on pressure drop of Taylor flow in capillaries. A.I.Ch.E. Journal 51 (9), 2428–2440.
Kumar, V., Vashisth, S., Hoarau, Y., Nigam, K.D.P., 2007. Slug flow in curved microreactors: hydrodynamic study. Chemical Engineering Science 62 (24), 7494–7504.
Lafaurie, B., Nardone, C., Scardovelli, R., Zaleski, S., Zanetti, G., 1994. Modelling merging and fragmentation in multiphase flows with SURFER. Journal of Computational Physics 113 (1), 134–147.
Lakehal, D., Larrignon, G., Narayanan, C., 2008. Computational heat transfer and two-phase flow topology in miniature tubes. Microfluidics and Nanofluidics 4 (4), 261–271.
Liu, D., Wang, S., 2008. Hydrodynamics of Taylor flow in noncircular capillaries. Chemical Engineering and Processing: Process Intensification 47 (12), 2098–2106.
Mishima, K., Hibiki, T., 1996. Some characteristics of air–water two-phase flow in small diameter vertical tubes. International Journal of Multiphase Flow 22 (4), 703–712.
Mishima, K., Hibiki, T., Nishihara, H., 1993. Some characteristics of gas–liquid flow in narrow rectangular ducts. International Journal of Multiphase Flow 19 (1), 115–124.
Ndinisa, N.V., Wiley, D.E., Fletcher, D.F., 2005. Computational fluid dynamics simulations of Taylor bubbles in tubular membranes model validation and application to laminar flow systems. Chemical Engineering Research and Design 83 (1 A), 40–49.
Pehlivan, K., Hassan, I., Vaillancourt, M., 2006. Experimental study on two-phase flow and pressure drop in millimeter-size channels. Applied Thermal Engineering 26 (14–15), 1506–1514.
Qian, D., Lawal, A., 2006. Numerical study on gas and liquid slugs for Taylor flow in a T-junction microchannel. Chemical Engineering Science 61 (23), 7609–7625.
Rosengarten, G., Harvie, D.J.E., Cooper-White, J., 2006. Contact angle effects on microdroplet deformation using CFD. Applied Mathematical Modelling 30, 1033–1042.
Saisorn, S., Wongwises, S., 2008. A review of two-phase gas–liquid adiabatic flow characteristics in micro-channels. Renewable and Sustainable Energy Reviews 12 (3), 824–838.
Salman, W., Gavriilidis, A., Angeli, P., 2006. On the formation of Taylor bubbles in small tubes. Chemical Engineering Science 61 (20), 6653–6666.
Serizawa, A., Feng, Z., Kawara, Z., 2002. Two-phase flow in microchannels. Experimental Thermal and Fluid Science 26 (6–7), 703–714.
Suo, M., Griffith, P., 1964. Two-phase flow in capillary tubes. Journal of Basic Engineering 86, 576–582.
Sussman, M., Smereka, P., Osher, S., 1994. A level set approach for computing solutions to incompressible two-phase flow. Journal of Computational Physics 114 (1), 146–159.
Taha, T., Cui, Z.F., 2002. CFD modelling of gas-sparged ultrafiltration in tubular membranes. Journal of Membrane Science 210 (1), 13–27.
Taha, T., Cui, Z.F., 2004. Hydrodynamics of slug flow inside capillaries. Chemical Engineering Science 59 (6), 1181–1190.
Taylor, G.I., 1960. Deposition of a viscous fluid on the wall of a tube. Journal of Fluid Mechanics 10, 161–165.
Thulasidas, T.C., Abraham, M.A., Cerro, R.L., 1997. Flow patterns in liquid slugs during bubble-train flow inside capillaries. Chemical Engineering Science 52 (17), 2947–2962.
Triplett, K.A., Ghiaasiaan, S.M., Abdel-Khalik, S.I., Sadowski, D.L., 1999. Gas–liquid two-phase flow in microchannels Part 1: two-phase flow patterns. International Journal of Multiphase Flow 25 (3), 377–394.
van Baten, J.M., Krishna, R., 2004. CFD simulations of mass transfer from Taylor bubbles rising in circular capillaries. Chemical Engineering Science 59 (12), 2535–2545.
van Baten, J.M., Krishna, R., 2005. CFD simulations of wall mass transfer for Taylor flow in circular capillaries. Chemical Engineering Science 60 (4), 1117–1126.
Yang, C.Y., Shieh, C.C., 2001. Flow pattern of air–water and two-phase R-134a in small circular tubes. International Journal of Multiphase Flow 27 (7), 1163–1177.
Youngs, D.L., 1982. Time-dependent multi-material flow with large fluid distortion. In: Morton, K.W., Baines, M.J. (Eds.), Numerical Methods for Fluid Dynamics. Academic, New York, pp. 273–285.
Yu, Z., Hemminger, O., Fan, L.-S., 2007. Experiment and lattice Boltzmann simulation of two-phase gas–liquid flows in microchannels. Chemical Engineering Science 62 (24), 7172–7183.
Zhao, T.S., Bi, Q.C., 2001. Co-current air–water two-phase flow patterns in vertical triangular microchannels. International Journal of Multiphase Flow 27 (5), 765–782.